Spectral Narrowing in Nonlinear Compton Scattering via Chirped Laser Pulses

Xiao-Hu Ji(吉小虎)[1], Aihua Liu(刘爱华)[2*], and Li-Guang Jiao(焦利光)[1*]

[1] *College of Physics, Jilin University, Changchun 130012, China*
[2] *Institute of Atomic and Molecular Physics, Jilin University, Changchun 130012, China*

(Received 13 January 2026; accepted manuscript online 18 March 2026)

Spectral broadening due to ponderomotive effects significantly limits the spectral brightness of light sources generated by nonlinear Compton scattering. In this study, within the strong-field quantum electrodynamics framework, we demonstrate that equal-power frequency-chirped laser pulses can significantly suppress spectral broadening by combining frequency modulation with temporal pulse extension. The resulting radiation energy is concentrated into a blue-shifted first-order harmonic with enhanced intensity and a near-symmetric angular distribution in the electron forward direction. The efficacy of the equal-power chirped lasers was examined in a high-energy regime involving ultra-relativistic electrons and super-intense laser fields. By contrast, an equal-full width at half maximum chirp, although convenient for theoretical studies, has a limited capability to suppress spectral broadening. Our findings establish an equal-power chirp as a practical and experimentally accessible method for spectral narrowing, thus offering an easy and viable route to enhance the spectral brightness of laser-driven Compton sources for generating narrow-band X-rays and γ-rays.

DOI: 10.1088/0256-307X/43/4/040304 CSTR: 32039.14.0256-307X.43.4.040304

1. Introduction. Advances in intense laser technology have enabled numerous nonlinear effects in laser–matter interactions, such as strong-field ionization,[1–3] high-order harmonic generation,[4,5] and nonlinear Compton scattering (NLC).[6–11] In a typical NLC process, a free electron scatters from an intense laser field with the coherent absorption of multiple photons and emits a single high-energy photon. The nonlinearity of NLC is characterized by the dimensionless parameter $\xi = |e|E\lambda_{\rm C}/(\hbar\omega)$,[8,9] where m is the electron mass; $\lambda_{\rm C} = \hbar/(mc)$ is the electron Compton wavelength; and E, λ, and ω denote the electric field amplitude, wavelength, and circular frequency of the laser field, respectively. The laser intensity for electron scattering is $I = \xi^2\,(\omega/\text{eV})^2 \times 8.9 \times 10^{17}\ \text{W/cm}^2$. Recent advances in laser technology have facilitated the experimental measurement of the photon emission spectra of NLC[12–19] and established them as a versatile platform for generating intense, narrow-band X-rays and γ-rays.[17–23] Recent interest in NLC has focused on the scattering of relativistic electrons with circularly polarized[24] or Laguerre–Gaussian[25–27] laser pulses to generate high-energy vortex photons, as well as with intense quantum light[28] to manipulate the radiation spectra with additional degrees of freedom from quantum light properties.

To obtain high-energy photons in NLC, one should increase the incident electron energy in general. For electron scattering with a fixed incident energy from a laser field with a definite energy flux density, the control and optimization of the energy- and angle-resolved photon emission spectra can be achieved not only by manipulating the phase space of the electron beam[29] but also by customizing the spatiotemporal profile of the laser field. The scattering of electrons with ultrashort intense laser pulses within the framework of quantum electrodynamics (QED) theory has been extensively investigated,[30–35] and the envelope of few-cycle pulses has been shown to govern the emitted photon spectrum. For example, Gaussian and sine-squared temporal envelopes split individual harmonics into multiple subpeaks, thus resulting in substantial spectral broadening known as ponderomotive broadening.[36–38] This deficiency arises from the envelope-induced drift of the electron quiver motion within the magnetic field of the laser pulse, with the number of subpeaks determined by both the pulse duration and peak intensity. Notably, merely extending the pulse duration without chirping does not eliminate these subpeaks, and obtaining an almost monochromatic spectrum requires a flat-top envelope, where the rising and falling edges of the pulse contribute negligibly to the photon emission.[32] Although generating ideal square-like pulses remains challenging experimentally, researchers have recently proposed promising schemes, such as the pulse-stacking technique,[39] to approximate rectangular envelopes in NLC.

In practical applications of NLC such as obtaining high-brightness X-ray sources, increasing the incident laser intensity is essential for enhancing the emitted photon flux. However, increasing the laser intensity increases ponderomotive broadening, thus imposing an inevitable limitation on the spectral brightness of the generated pulses. This limitation has been clearly observed in NLC experiments with large values of ξ,[14–17] thus rendering the suppression of spectral broadening a critical issue. Applying frequency chirps to the driving laser field offers a practical approach for mitigating ponderomotive broadening. Based

*Corresponding authors. Email: aihualiu@jlu.edu.cn; lgjiao@jlu.edu.cn
© 2026 Chinese Physical Society and IOP Publishing Ltd. All rights, including for text and data mining, AI training, and similar technologies, are reserved.

on strong-field QED theory, Seipt *et al.*[40,41] successfully derived a highly nonlinear temporal chirp that can maximally suppress ponderomotive broadening at a specified photon emission angle. However, the complex functional form of the analytical solution renders its experimental realization challenging. Recently, catastrophe theory was combined with numerical scanning techniques to identify chirp parameters that maintain a good balance between optimal performance and experimental feasibility, thus facilitating the development of practical light sources based on theoretical predictions.[42,43]

In this study, we investigate the efficacy of two types of frequency-chirped Gaussian laser pulses for suppressing ponderomotive broadening in NLC. Our investigation reveals that an equal-power chirp can effectively suppress spectral broadening and focus radiation in the forward electron direction, whereas an equal-full width at half maximum (FWHM) chirp only disorders the spectra by breaking the angular symmetry of radiation. The Feynman slash notation, $\not{a} = \gamma_\mu a^\mu$, light-cone coordinates $a^\pm = a_0 \pm a_z$, the metric $g^{\mu\nu} = \mathrm{diag}(+1,-1,-1,-1)$, and Lorentz-Heaviside units with $\hbar = c = \mu_0 = 1$ are used herein.

2. Theoretical Method. The NLC process of electron scattering from an intense laser field is modeled within the framework of strong-field QED theory in the Furry picture,[44] where the interaction between the electron and laser field is modeled non-perturbatively, whereas the photon emission process is treated perturbatively. We considered the head-on collision geometry illustrated in Fig. 1. The laser pulse propagates along the positive z-axis with momentum $k = \omega_0 n$, where $n = (1,0,0,1)$ and ω_0 is the laser center frequency. The laser phase is defined as $\phi = k^\mu x_\mu = \omega_0(t-z)$. The electron is initialized by moving along the negative z-axis with momentum $p^\mu = (m\gamma, 0, 0, -m\sqrt{\gamma^2-1})$, in which γ is the Lorentz factor. In this study, we set $\gamma = 2$, which corresponds to an incident electron with an energy of approximately 1 MeV. The leading order of the S-matrix for single-photon emissions is expressed as[8,9]

$$S_{fi} = -\mathrm{i}e \int \bar{\psi}_{p'} \not{\varepsilon}'^{*}_{\lambda'} \mathrm{e}^{\mathrm{i}k'x} \psi_p \mathrm{d}^4 x, \tag{1}$$

where p, p', and k' are the four-momenta for the initial electron, final electron, and emitted photon, respectively; and $\varepsilon'_{\lambda'}$ represents the polarization vector of the emitted photon. Free electron states ψ_p propagating in an external electromagnetic field are described by the Volkov state.[45] Here, we focus on the energy- and angle-resolved photon emission spectra. Within the standard strong-field QED procedure, the differential spectrum is expressed as[8,9]

$$\frac{\mathrm{d}E}{\mathrm{d}\omega' \mathrm{d}\Omega} = \frac{e^2 \omega'^2}{16(2\pi)^3 p^- p'^- \omega_0^2} \sum_{\lambda'} \left(\mathrm{tr}\left[\not{p} \mathcal{Z} \not{p}' \bar{\mathcal{Z}} \right] + m^2 \,\mathrm{tr}[\mathcal{Z}\bar{\mathcal{Z}}] \right). \tag{2}$$

The detailed expression for the matrix $\mathcal{Z}$ is provided in the Supplementary Material. The spectrum derived above is a function of the emitted photon energy ω' and solid angle Ω, from which the emitted photon momentum k' can be defined. A linearly polarized laser pulse with a Gaussian envelop is employed in this study and its four-vector potential is expressed as $A^\mu(\phi) = A_0 F(\phi)\,\mathrm{Re}[\mathrm{e}^{\mathrm{i}f(\phi)}\varepsilon^\mu]$, where $F(\phi)$ is the pulse envelope, $\varepsilon^\mu = (0,1,0,0)$ the polarization vector, and $f(\phi)$ the temporal phase profile from which the frequency chirp can be incorporated. For a monochromatic plane-wave laser, $F(\phi) = 1$ and $f(\phi) = \phi$. In this study, we consider two distinct forms of chirped laser pulses. The first form, which is referred to as the equal-FWHM chirp, maintains a constant FWHM independent of the chirp parameter.[46–49] The corresponding laser parameters are $A_0 = m\xi/e$, $F(\phi) = \exp(-2(\ln 2)\phi^2/\tau_0^2)$, and $f(\phi) = \phi + 4(\ln 2) b\phi^2/\tau_0^2 + \phi_{\mathrm{cep}}$, where b is the chirp parameter, ϕ_{cep} the carrier-envelope phase, and τ_0 the pulse duration. The second form, termed the equal-power chirp, maintains a constant power spectral distribution by varying the chirp parameter b.[43,49–55] The laser parameters are $A_0 = m\xi/(e(1+b^2)^{1/4})$, $F(\phi) = \exp(-2(\ln 2)\phi^2/(\tau_0^2(1+b^2)))$, and $f(\phi) = \phi + 2(\ln 2)\phi^2 b/(\tau_0^2(1+b^2)) + \phi_{\mathrm{cep}}$. The properties of these two chirped pulses are analyzed in detail in the Supplementary Material. In this study, unless otherwise mentioned, we employed the following laser parameters: $\tau_0 = 10$, $\xi = 1.5$ (corresponds to the laser intensity of $I = 4.811 \times 10^{18}\,\mathrm{W/cm^2}$), $\phi_{\mathrm{cep}} = \pi/2$, and $\omega_0 = 1.55\,\mathrm{eV}$ (laser wavelength of 800 nm). These parameters were selected within the accessible range of current NLC experiments.

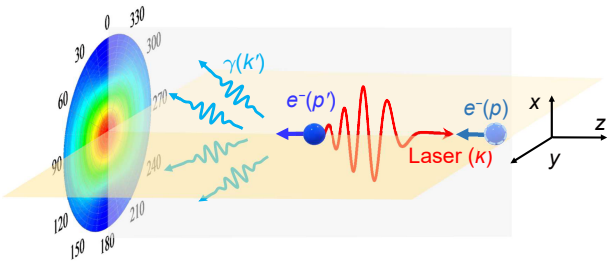

Fig. 1. Schematic diagram of nonlinear Compton scattering. Incident electron propagates along negative z-axis with four-momentum p and head-on collides with a counter-propagating, linearly polarized chirped laser pulse with wave four-vector k. Scattered electron and emitted photon have four-momenta p' and k', respectively. Photon is radiated at a polar angle θ with respect to the z-axis. Total radiation spectrum is illustrated on the left.

3. Results and Discussion. First, the spectral pattern in the chirp-free ($b = 0$) condition is analyzed. The observation direction is restricted to the x–z plane, which implies that the differential photon emission spectrum expressed in Eq. (2) is a function of ω' and $\theta \in [0°, 360°]$. The calculated results for $\gamma = 2$ are presented in Fig. 2(a). A distinct feature of the spectrum is that the photon emission direction is focused primarily at approximately $\theta = 180°$, with multipeak structures in the energy-resolved spectrum indicating high-order harmonic generation. The harmonic order can be identified by employing the analytical expression of emitted photon energy as a function of laser phase under the approximation of gradually varying envelope,[40]

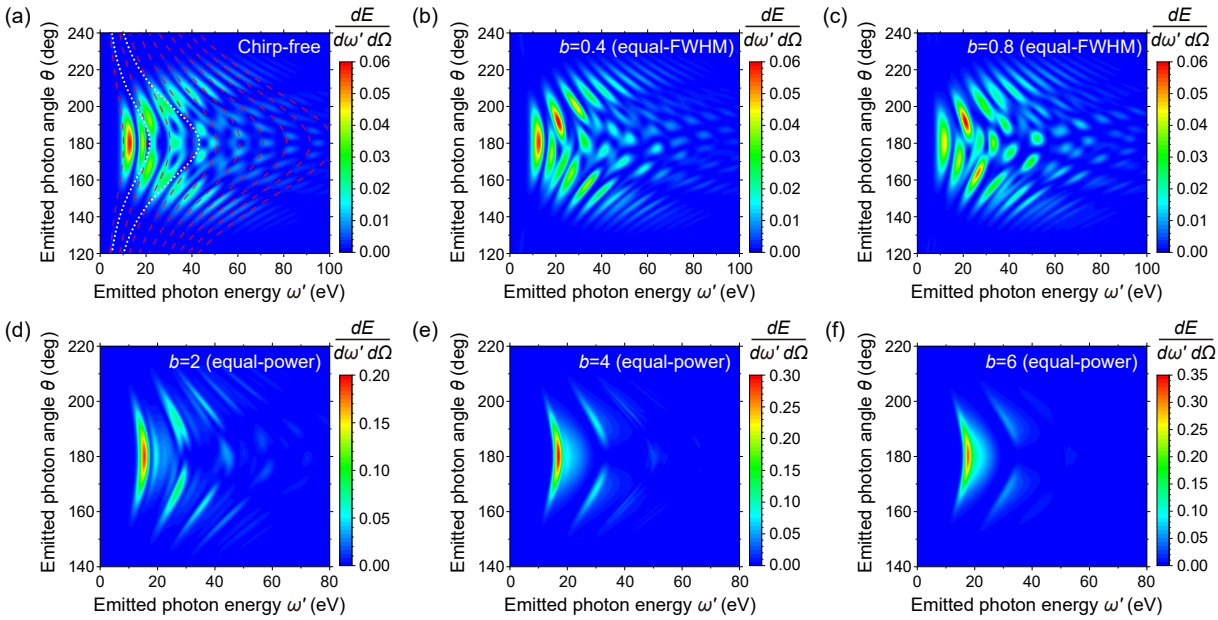

Fig. 2. Photon emission spectra $\mathrm{d}E/(\mathrm{d}\omega'\mathrm{d}\Omega)$ for chirp-free Gaussian laser pulse (a), equal-FWHM chirped laser pulses with $b = 0.4$ (b) and 0.8 (c), and equal-power chirped laser pulses with $b = 2$ (d), 4 (e), and 6 (f). All spectra are observed in x–z plane and $\theta = 180°$ refers to electron forward direction.

i.e., $\omega'(\phi) = \ell(pk)/\left[(p + U(\phi) + \ell k)n'\right]$, where $U(\phi) = m^2\xi^2F^2(\phi)k/(4pk)$ is the ponderomotive four-vector potential of the electron, ℓ the number of absorbed photons, and $n' = (1, \sin\theta\cos\varphi, \sin\theta\sin\varphi, \cos\theta)$ the unit four-vector indicating the photon emission direction. Based on the equation above, the envelope function $F(\phi)$ induces a phase-dependent modulation of the effective electron mass, thus resulting in a spectral shift that depends on the laser phase. At the pulse rising and falling edges, where $F(\phi) \approx 0$, the system approached the conventional Compton scattering regime, thereby yielding a maximum photon energy of $\omega'_{\mathrm{max},\ell} = \ell(pk)/\left[(p + \ell k)n'\right]$ for the ℓth-order harmonic. By contrast, at the pulse peak where $F(\phi) = 1$, the ponderomotive potential reached its maximum; consequently, the ℓth-order harmonic minimum photon energy can be expressed as $\omega'_{\mathrm{min},\ell} = \ell(pk)/\left[(p + m^2\xi^2/(4pk)k + \ell k)n'\right]$. Notably, this minimum photon energy coincides exactly with the monochromatic plane-wave results[9] at $F(\phi) = 1$ and $f(\phi) = \phi$. The spectral boundaries of ponderomotive broadening are clearly visible in Fig. 2(a), where the 10 dashed red lines indicate $\omega'_{\mathrm{min},\ell}$ for the harmonics of $\ell = 1$ to 10 from left to right, and the two dotted white lines refer to $\omega'_{\mathrm{max},\ell}$ with $\ell = 1$ and 2. The first-order harmonic exhibited a double-peak structure, with the primary and secondary peaks located at approximately $\omega' = 13.0$ and 18.5 eV, respectively. The entire first-order harmonic spectrum was well-bounded by the theoretical predictions of $\omega'_{\mathrm{min},\ell=1}$ and $\omega'_{\mathrm{max},\ell=1}$. This feature clearly indicates that a first-order harmonic photon was emitted across the entire temporal profile of the laser pulse. By contrast, higher-order harmonics with $\ell \geq 2$ were primarily concentrated near $\omega'_{\mathrm{min},\ell}$, thus indicating that they were predominantly emitted during the laser peak intensity. This is consistent with the strong-field approximation, which states that higher-order nonlinear processes are accessible by stronger laser fields. Spectral broadening, together with the characteristic splitting of each harmonic, constitute ponderomotive broadening in the NLC photon emission spectra, which inherently limits the spectral brightness of the generated coherent light sources.

For comparison, we first employed equal-FWHM chirped pulses. The corresponding photon emission spectra at $b = 0.4$ and 0.8 are presented in Figs. 2(b) and 2(c), respectively. A comparison with the chirp-free results shown in Fig. 2(a) reveals a persistent splitting and disordering of harmonic peaks, thus indicating the limited capability of the equal-FWHM chirp in suppressing ponderomotive broadening. Even at the maximum chirp parameter of $b = 0.8$, where the smallest instantaneous frequency approaches zero, the characteristic multi-peak structures remain clearly visible. The use of equal-FWHM chirps breaks the fundamental symmetry of the scattering system. In the chirp-free case, the emission spectrum is symmetric with respect to the electron forward direction at $\theta = 180°$. From a classical perspective, the central symmetry of the laser field implies symmetric radiation patterns and intensities for $\theta < 180°$ and $\theta > 180°$. However, as shown in Fig. S1(a) in the Supplementary Material, the equal-FWHM chirp destroys the central symmetry of the laser temporal profile, thus resulting in distinctly asymmetric photon emission spectra, as shown in Figs. 2(b) and 2(c). The results for the negative chirp parameters of $b < 0$ were the same as those for $b > 0$ after the spectra was inverted with respect to $\theta = 180°$. Thus, they are excluded for brevity.

The photon emission spectra driven by equal-power chirped laser pulses are shown in Figs. 2(d), 2(e), and 2(f) at chirp parameters of $b = 2$, 4, and 6, respectively. In contrast to the equal-FWHM case, the photon emission spectra driven by equal-power chirped pulses generally

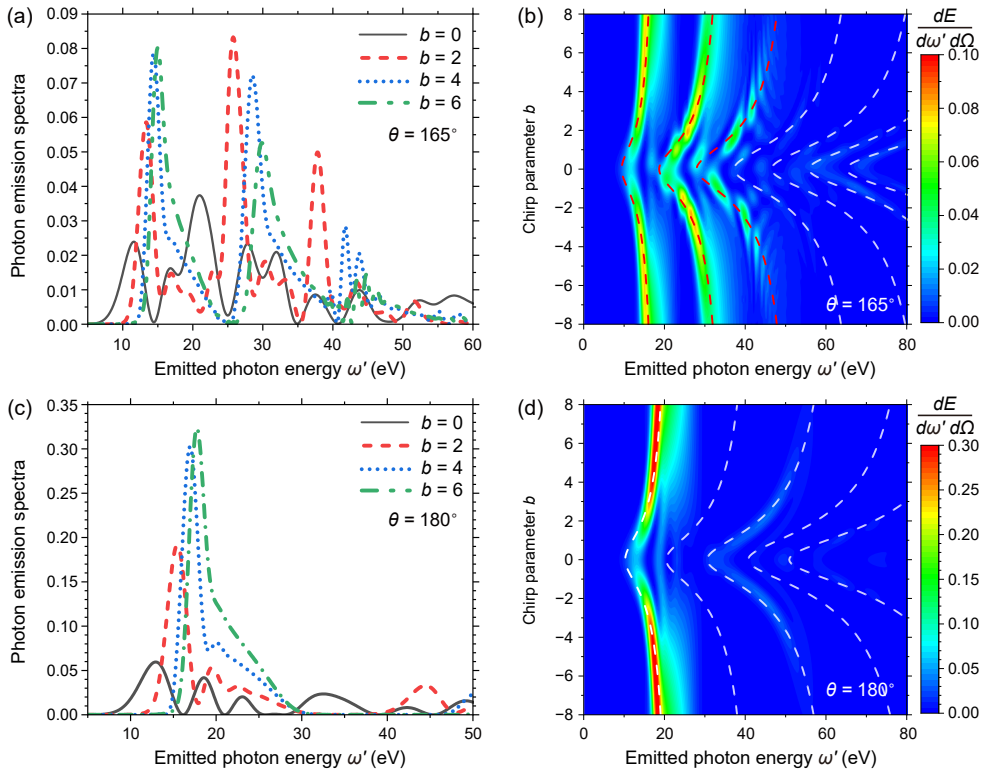

Fig. 3. Photon emission spectra as a function of emitted photon energy and equal-power chirp parameter. Photon emission angle is $\theta = 165°$ for panels (a) and (b) and $\theta = 180°$ for panels (c) and (d), respectively.

maintained the inversion symmetry of the pattern with respect to $\theta = 180°$. This is because the equal-power chirp does not significantly disrupt the central symmetry of the laser pulse, as shown in Fig. S1(c) in the Supplementary Material. Strong enhancement in the radiation intensity at low-order harmonics was observed as the chirp parameter increased, even though the peak laser intensity decreased considerably. This counterintuitive behavior can be explained by the concurrent temporal extension of the laser pulse. The longer duration of the laser-electron interaction compensates for the reduced peak field intensity, thus resulting in a net increase in the radiation intensity at low-order harmonics. More importantly, the equal-power chirp excelled at suppressing ponderomotive broadening. This is because the frequency chirp reduces the laser intensity, which further decreases the nonlinear parameter. Using Eq. (S15) in the Supplementary Material, we can define an effective chirp-dependent nonlinear parameter $\xi_{\text{eff}} = \xi/(1 + b^2)^{1/4}$, from which we can define the effective chirp-dependent ponderomotive potential $U_{\text{eff}}(\phi) = m^2\xi_{\text{eff}}^2 F^2(\phi)k/(4pk)$. An increase in the chirp parameter b gradually decreases the ponderomotive potential, thereby suppressing spectral broadening. Another phenomenon that can be observe from Figs. 2(a), 2(d), 2(e), and 2(f) is that, as the chirp parameter increased, the multipeak structure in the unchirped spectrum gradually merged into distinct harmonics and the emitted photon energies concentrated primarily in the first- and second-order harmonic channels. The multipeak structure in the unchirped spectrum originates from the interference between photons emitted at the rising and falling edges of the pulse, owing to the temporal symmetry of the laser pulse. The introduction of a frequency chirp breaks such symmetry and, therefore, eliminates temporal interference and discrete interference fringes. These spectral narrowing and purification effects represent crucial advantages of equal-power chirped lasers in applications requiring high spectral brightness. To further understand the different roles of temporal pulse extension and frequency modulation in equal-power chirped lasers, we include a comparative analysis of a control case in the Supplementary Material. By comparing with a reference pulse having the same peak intensity and duration but without a frequency chirp, we demonstrate that whereas the narrowing of the radiation spectral range is primarily attributed to a reduction in laser intensity and an extension of the pulse duration, the role of frequency modulation is equally important. Its unique advantage is its ability to suppress spectral fragmentation by eliminating the interference between emissions at different times and enabling the effective control of ponderomotive broadening without changing the laser spectrum.

To characterize the spectral narrowing effect of equal-power chirped pulses quantitatively, we analyze the radiation spectra at fixed detection angles. Figure 3(a) presents the photon emission spectra at $\theta = 165°$ for chirp parameters $b = 0$, 2, 4, and 6. As b increased, the multiple subpeaks within each harmonic merged progressively, thus resulting in significantly narrower spectral peaks. The merging of the spectral subpeaks was accompanied by a systematic blue shift in the harmonic energies. A complete evolution of the spectra at $\theta = 165°$ for $-8 \le b \le 8$

is shown in Fig. 3(b), which presents the radiation intensity as a function of the photon energy and chirp parameter. The spectra were generally insensitive to the sign of the chirp parameter, which depends primarily on its magnitude. As the chirp parameter increased, the peaks of the radiation spectra for different harmonics shifted toward higher energies, and this blue shift eventually saturated for large chirp parameters. This behavior can be similarly understood based on the effective nonlinear parameter $\xi_{\text{eff}} = \xi/(1+b^2)^{1/4}$. Substituting it into the minimum emitted photon energy for the ℓth-order harmonic yields $\omega'_{\text{min},\ell}(b) = \ell(pk)/\left(p + m^2\xi^2 k/\left(4(pk)\sqrt{1+b^2}\right) + \ell k\right) n'$. The dashed lines in Fig. 3(b) provide visual guidance to the approximate predictions above. As shown, the predictions agreed well with the numerical calculations at least for the first three orders of harmonics. Figures 3(c) and 3(d) show the photon emission spectra at the electron forward direction of $\theta = 180°$. The radiation intensity of the first-order harmonics improved significantly as the chirp parameter increased, whereas the even-order harmonics were completely suppressed because of the symmetry constraint. The observed spectral peaks aligned well with the theoretical predictions of $\omega'_{\text{min},\ell}$ (dashed lines), thus demonstrating the successful suppression of ponderomotive broadening through the equal-power chirped pulses. This emission-angle dependence of spectral focusing and narrowing highlights the geometric sensitivity of the chirp compensation mechanism and its significant relationship with the collision dynamics.

To better illustrate the spectral narrowing effect of the equal-power chirped pulses, we integrated the photon emission spectrum $\mathrm{d}E/(\mathrm{d}\omega'\mathrm{d}\Omega)$ over the emitted photon energy ω' to obtain the angular distribution of radiation energy $\mathrm{d}E/\mathrm{d}\Omega$. The results are shown in Fig. 4 for $b = 0$, 2, 4, and 6. The angular distributions were symmetric about $\theta = 180°$. As the chirp parameter increased gradually, the angular distribution became more concentrated in the electron forward direction. This focusing effect is due to the suppression of higher-order harmonic generations emitted into a broader angular cone. A larger chirp parameter results in a narrower angular distribution of photon energy. Additionally, figure 4 shows the calculation results obtained using an equal-FWHM chirped pulse at $b = 0.8$. An angular distribution that is almost identical to that of the unchirped case is shown. Therefore, the equal-FWHM chirp did not exhibit a spectral focusing effect. Finally, the total radiated photon energy remained unchanged for different chirp parameters under both equal-power and equal-FWHM chirped pulses. This total photon energy, which was obtained by integrating $\mathrm{d}E/\mathrm{d}\Omega$ over the full solid angle Ω, was approximately 0.7 eV for the electron and laser parameters used currently. We conclude that both chirp models modify the energy and angular distributions of the emitted radiation without altering the total energy transferred during Compton scattering.

Finally, we evaluated the performance of the equal-power chirp in the ultra-relativistic regime, where high-energy photons were generated. We considered the scattering of a 5 GeV electron (Lorentz factor of $\gamma = 10^4$) from a super-intense laser pulse of central frequency $\omega_0 = 15.5$ eV (laser wavelength of 80 nm). The nonlinear parameter was selected as $\xi = 3$, which corresponds to a laser field intensity of $I = 1.924 \times 10^{21}$ W/cm^2. All of these parameters are accessible in the current experimental facilities.[56–59] In this regime, the radiation emission became highly directional and concentrated primarily along the initial direction of the incident electron. Therefore, our analysis should be restricted to $\theta = 180°$. Figure 5 shows the calculated photon emission spectra for equal-power chirped laser pulses with $b = 0$, 2, 4, 8, and 14. At such a high laser intensity, the unchirped and weakly chirped spectra shown in Fig. 5(a) exhibited intricate complexities, with each harmonic fragmenting into numerous subpeaks owing to the strong ponderomotive modulation. Additionally, under these laser parameters, the recoil of the emitted photons became non-negligible, thus causing the photon emission spectra to be cutoff at $\omega' = 4.7$ GeV. The photon recoil effect requires a full quantum treatment of the photon emission and cannot be treated within the classical electrodynamics theory. Based on Fig. 5(a), setting $b = 2$ is insufficient to suppress the pronounced ponderomotive broadening. Under a continuously increasing b, as shown in Fig. 5(b), chirped pulses with b values larger than 8 successfully focused the spectra. The radiated photon energy, which was previously distributed across multiple harmonic structures, concentrated predominantly in the first order, with an energy well-predicted by $\omega'_{\text{min},\ell}$ with $\ell = 1$. The successful suppression of ponderomotive broadening in the ultra-relativistic electron and super-intense laser regime validated that the equal-power chirp remained effective when extended to extreme conditions. Thus, it provides a practical route for generating narrow-band high-brightness radiations, thus contributing to the advancement of compact X-ray and γ-ray sources in NLC experiments.

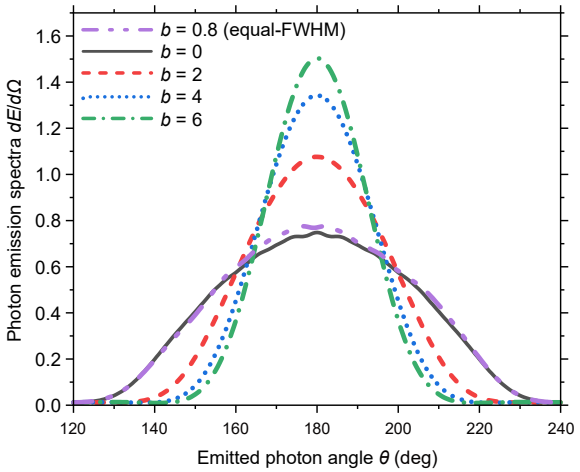

Fig. 4. Angular distribution of radiation energy $\mathrm{d}E/\mathrm{d}\Omega$ obtained by integrating spectra in Fig. 2 over emitted photon energy ω'. Equal-power chirped pulses with $b = 0$, 2, 4, and 6 are shown and only equal-FWHM chirped pulse with $b = 0.8$ is included for comparison.

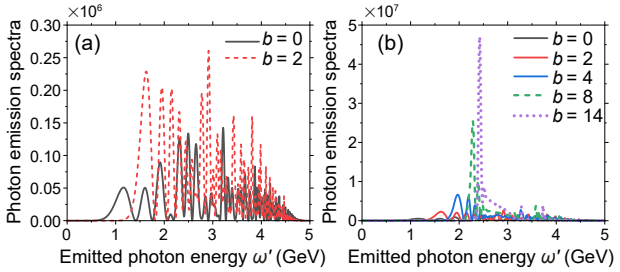

Fig. 5. High-energy photon emission spectra at $\theta = 180°$ as a function of emitted photon energy for $\gamma = 10^4$, $\xi = 3$, and $\omega_0 = 15.5\,\text{eV}$. Equal-power chirped lasers with $b = 0$ and 2 are shown in panel (a) and with b as large as 14 in panel (b).

4. Conclusion. Within the framework of strong-field QED theory, we systematically examined the effect of frequency-chirped laser pulses on the photon emission spectra in NLC. Two distinct chirp models were considered. An equal-FWHM chirp offered limited capability in suppressing spectral broadening and destroyed the central symmetry of the emission pattern. By contrast, an equal-power chirp effectively combined the complementary mechanisms of frequency modulation and compensatory temporal pulse extension. This dual effect significantly reduced the ponderomotive broadening of few-cycle laser pulses, thus resulting in spectral focusing and narrowing, where the radiation energy was concentrated predominantly in the blue-shifted first-order harmonic in the electron forward direction. More importantly, the equal-power chirp preserved the angular symmetry of the photon emission and remained robust under extreme conditions involving ultra-relativistic electrons and super-intense laser fields. Our findings established equal-power chirps as a viable and experimentally practical approach for enhancing spectral control and improving spectral quality in laser-driven Compton sources. Additionally, this methodology provides a direct pathway for generating narrowband, high-brightness light sources based on laser-electron scattering.

5. Acknowledgements. This study was supported by the National Key Research and Development Program of China (Grant No. 2022YFE0134200), the National Natural Science Foundation of China (Grant Nos. 12474343 and 12174147), and the Graduate Innovation Fund of Jilin University (Grant No. 2024KC048).

References

[1] Mourou G 2019 *Rev. Mod. Phys.* **91** 030501
[2] Xiao F, Wang L, Bai G *et al.* 2025 *Chin. Phys. Lett.* **42** 043701
[3] Luo X, Ji X, Jiao L, Liu A, and Liu X 2025 *Chin. Phys. Lett.* **42** 070301
[4] L'Huillier A 2024 *Rev. Mod. Phys.* **96** 030503
[5] Wang L, Wang X, Xiao F, Wang J, Tao W, Zhang D, and Zhao Z 2023 *Chin. Phys. Lett.* **40** 113201
[6] Fedotov A, Ilderton A, Karbstein F, King B, Seipt D, Taya H, and Torgrimsson G 2023 *Phys. Rep.* **1010** 1
[7] King B and Tang S 2020 *Phys. Rev. A* **102** 022809
[8] Shao Z Q, Dong Q L, Yue D N, Teng H, Wei Z Y, Chen M, and Zhang J 2024 *Phys. Rev. A* **110** 033117
[9] Mackenroth K F 2014 *Quantum Radiation in Ultra-Intense Laser Pulses* (Springer Cham)
[10] Zhao L, Chen Z J, Sang H B, and Xie B S 2019 *Chin. Phys. Lett.* **36** 074101
[11] Zhang Y, Mo C, Zhang P, and Kang W 2024 *Chin. Phys. Lett.* **41** 017801
[12] Hou R, Zhang W, Han X, Wang H F, and Zhang S 2025 *Chin. Phys. Lett.* **42** 014203
[13] An F, Bai D, Cai H J *et al.* 2025 *Chin. Phys. Lett.* **42** 110102
[14] Sarri G, Corvan D J, Schumaker W *et al.* 2014 *Phys. Rev. Lett.* **113** 224801
[15] Khrennikov K, Wenz J, Buck A, Xu J, Heigoldt M, Veisz L, and Karsch S 2015 *Phys. Rev. Lett.* **114** 195003
[16] Cole J M, Behm K T, Gerstmayr E *et al.* 2018 *Phys. Rev. X* **8** 011020
[17] Chen S, Powers N D, Ghebregziabher I *et al.* 2013 *Phys. Rev. Lett.* **110** 155003
[18] Albert F, Anderson S G, Gibson D J *et al.* 2010 *Phys. Rev. ST Accel. Beams* **13** 070704
[19] Albert F, Anderson S G, Gibson D J, Marsh R A, Wu S S, Siders C W, Barty C P J, and Hartemann F V 2011 *Phys. Rev. ST Accel. Beams* **14** 050703
[20] Gales S, Tanaka K A, Balabanski D L *et al.* 2018 *Rep. Prog. Phys.* **81** 094301
[21] Krämer J M, Jochmann A, Budde M *et al.* 2018 *Sci. Rep.* **8** 1398
[22] Karagodsky V and Schächter L 2011 *Plasma Phys. Control. Fusion* **53** 014007
[23] Geddes C G, Rykovanov S, Matlis N H *et al.* 2015 *Nucl. Instrum. Methods Phys. Res. Sect. B* **350** 116
[24] Ababekri M, Guo R T, Wan F, Qiao B, Li Z, Lv C, Zhang B, Zhou W, Gu Y, and Li J X 2024 *Phys. Rev. D* **109** 016005
[25] Ju L, Zhou C, Huang T, Jiang K, Wu C, Long T, Li L, Zhang H, Yu M, and Ruan S 2019 *Phys. Rev. Appl.* **12** 014054
[26] Bogdanov O, Kazinski P, and Lazarenko G 2019 *Phys. Rev. D* **99** 116016
[27] Jiang J J, Zhuang K H, Chen J D, Li J X, and Chen Y Y 2025 *Phys. Rev. Lett.* **134** 153802
[28] Khalaf M and Kaminer I 2023 *Sci. Adv.* **9** eade0932
[29] Krafft G A, Terzić B, Johnson E, and Wilson G 2023 *Phys. Rev. Accel. Beams* **26** 034401
[30] Boca M and Florescu V 2009 *Phys. Rev. A* **80** 053403
[31] Heinzl T, Seipt D, and Kämpfer B 2010 *Phys. Rev. A* **81** 022125
[32] Seipt D and Kämpfer B 2011 *Phys. Rev. A* **83** 022101
[33] Krajewska K and Kamiński J Z 2012 *Phys. Rev. A* **85** 062102
[34] Andreev O Y, Yu D, Lyashchenko K N, and Vasileva D M 2025 *Chin. Phys. Lett.* **42** 090301
[35] Wang N, Jiao L, and Liu A 2019 *Chin. Phys. B* **28** 093402
[36] Krafft G 2004 *Phys. Rev. Lett.* **92** 204802
[37] Hartemann F V, Albert F, Siders C W, and Barty C P 2010 *Phys. Rev. Lett.* **105** 130801
[38] Kharin V Y, Seipt D, and Rykovanov S G 2016 *Phys. Rev. A* **93** 063801
[39] Timoshenko A, Malakhov M, Fedotov A, and Rykovanov S 2025 *Phys. Rev. A* **112** L061501
[40] Seipt D, Rykovanov S G, Surzhykov A, and Fritzsche S 2015 *Phys. Rev. A* **91** 033402
[41] Seipt D, Kharin V Y, and Rykovanov S G 2019 *Phys. Rev. Lett.* **122** 204802
[42] Kharin V Y, Seipt D, and Rykovanov S G 2018 *Phys. Rev. Lett.* **120** 044802
[43] Valialshchikov M A, Seipt D, Kharin V Y, and Rykovanov S G 2022 *Phys. Rev. A* **106** L031501
[44] Furry W H 1951 *Phys. Rev.* **81** 115
[45] Wolkow D M 1935 *Z. Phys.* **94** 250

[46] Barmaki S, Lanteigne P, and Laulan S 2014 *Phys. Rev. A* **89** 063406

[47] Wang N and Liu A 2019 *Chin. Phys. B* **28** 083403

[48] Fang Y K, Geng L, and Peng L Y 2014 *Phys. Rev. A* **109** 013113

[49] Zhu F, Liu X, Gao Y, Wang N, Jiao L, and Liu A 2021 *Chin. Phys. B* **30** 094209

[50] Tong Y, Jiang W C, Wu P, and Peng L Y 2016 *Chin. Phys. B* **25** 073202

[51] Peng L Y, Tan F, Gong Q, Pronin E A, and Starace A F 2009 *Phys. Rev. A* **80** 013407

[52] Ni Y Y, Zhao S F, Li X Y, Wang G L, and Zhou X X 2018 *Chin. Phys. B* **27** 073203

[53] Zille D, Adolph D, Möller M, Sayler A M, and Paulus G G 2018 *New J. Phys.* **20** 063018

[54] Yusoff M A H B M and Djiokap J M N 2024 *Phys. Rev. A* **109** 023107

[55] Zhao H, Liu C, Zheng Y, Zeng Z, and Li R 2017 *Opt. Express* **25** 7707

[56] Gonsalves A J, Nakamura K, Daniels J *et al.* 2019 *Phys. Rev. Lett.* **122** 084801

[57] Yoon J W, Kim Y G, Choi I W, Sung J H, Lee H W, Lee S K, and Nam C H 2021 *Optica* **8** 630

[58] Permogorov A, Cantono G, Guenot D, Persson A, and Wahlström C G 2022 *Sci. Rep.* **12** 3031

[59] Froula D H, Turnbull D, Davies A S *et al.* 2018 *Nat. Photon.* **12** 262